

# Perturbation theory for nonlinear halo power spectrum: the renormalized bias and halo bias

Atsushi J. Nishizawa<sup>\*</sup>, Masahiro Takada and Takahiro Nishimichi

*Kavli Institute for the Physics and Mathematics of the Universe (Kavli IPMU, WPI), The University of Tokyo, Chiba 277-8582, Japan*

12 June 2021

## ABSTRACT

We revisit an analytical model to describe the halo-matter cross-power spectrum and the halo auto-power spectrum in the weakly nonlinear regime, by combining the perturbation theory (PT) for matter clustering, the local bias model, and the halo bias. Nonlinearities in the power spectra arise from the nonlinear clustering of matter as well as the nonlinear relation between the matter and halo density fields. By using the “renormalization” approach, we express the nonlinear power spectra by a sum of the two contributions: the nonlinear matter power spectrum with the effective linear bias parameter, and the higher-order PT spectra having the halo bias parameters as the coefficients. The halo auto-power spectrum includes the residual shot noise contamination that needs to be treated as additional free parameter. The higher-order PT spectra and the residual shot noise cause a scale-dependent bias function relative to the nonlinear matter power spectrum in the weakly nonlinear regime. We show that the model predictions are in good agreement with the spectra measured from a suit of high-resolution  $N$ -body simulations up to  $k \approx 0.2 \text{ hMpc}^{-1}$  at  $z = 0.35$ , for different halo mass bins.

**Key words:** galaxies: clusters: general – cosmology: theory – dark energy – large-scale structure of Universe

## 1 INTRODUCTION

Clustering statistics of galaxies such as the two-point correlation function of galaxies or the Fourier-transformed-counterpart power spectrum are powerful tools to constrain cosmology. In particular, the baryon acoustic oscillation (BAO) experiment with wide-area galaxy redshift survey is recognized as a robust probe of cosmological distances. There are various on-going and planned galaxy surveys aimed at achieving high-precision BAO measurements over a wider range of redshifts: the SDSS-III Baryon Oscillation Spectroscopic Survey (BOSS)<sup>1</sup>, Subaru Prime Focus Spectrograph (PFS) Survey<sup>2</sup>, and the ESA Euclid satellite experiment<sup>3</sup>.

The BAO scale is one particular length scale measured from the pattern of galaxy clustering. Much more significant signal-to-noise ratios are inherent in the broad-band shape and amplitude information of the galaxy power spectrum at BAO scales. However, to reliably use the amplitude information, we need to resolve various systematic uncertainties in the weakly nonlinear regime: the nonlinear clustering effect and galaxy bias uncertainty. There are promising developments towards a more accurate modeling of the nonlinear clustering of matter based on  $N$ -body simulations (Springel et al. 2005; Angulo et al. 2008; Takahashi et al. 2009;

Nishimichi et al. 2009; Valageas & Nishimichi 2011) as well as perturbation theory (PT) of structure formation (Juszkiewicz 1981; Vishniac 1983; Makino et al. 1992; Jain & Bertschinger 1994; Jeong & Komatsu 2006; Crocce & Scoccimarro 2006; Matsubara 2008a; Taruya & Hiramatsu 2008; Saito et al. 2008; Nishimichi et al. 2007).

The galaxy bias uncertainty is a harder problem, because physical processes involved in galaxy formation/evolution are highly nonlinear and still very challenging to model from the first principles. Hence a practical approach often used assumes an empirical parametrization of galaxy bias; the peak bias model (Kaiser 1984; Mo & White 1996; Sheth & Tormen 1999; Schmidt et al. 2012) and the local bias model assuming a “local” mapping relation between galaxy and matter distributions at each spatial position (Coles 1993; Fry & Gaztanaga 1993; Scherrer & Weinberg 1998; Schmidt et al. 2012). In the peak bias model, a galaxy or more precisely halo is assumed to form at or around the peak of the initial matter density field, where a typical scale of the peaks corresponds to scales of the halo that host galaxies at low redshifts (although one halo can contain several galaxies inside). Thus the distribution of halos are by nature biased relative to the underlying matter distribution (Kaiser 1984), because only the density peaks can be places to have halos today, while the under-density regions or the density minima are very difficult (or impossible) to form halos. Furthermore, the long-wavelength perturbation mode in the initial density field causes modulations in the heights of the small-scale peaks, and in turn alter subsequent formation of halos at low redshifts. The amount

<sup>\*</sup> email: atsushi.nishizawa@ipmu.jp

<sup>1</sup> <http://www.sdss3.org/surveys/boos.php>

<sup>2</sup> <http://sumire.ipmu.jp/en/2652>

<sup>3</sup> <http://sci.esa.int/science-e/www/area/index.cfm?fareaid=102>

of halo bias can depend on the long-wavelength modes as a result of mode coupling in the weakly nonlinear regime relevant for BAO scales. The halo bias or peak bias models have been studied in the literature (Mo & White 1996; Sheth & Tormen 1999; Desjacques et al. 2011; Scoccimarro et al. 2012; Schmidt et al. 2012).

The nonlinear effect on the galaxy power spectrum arises from two effects: the nonlinear clustering of matter (mostly dark matter) and the nonlinear bias relation between the galaxy and dark matter distributions. At BAO scales in the weakly nonlinear regime, we expect that the nonlinear clustering of galaxies can be accurately modeled by incorporating the PT of structure formation, the local bias model and/or the peak-background split bias model (halo bias). Such an attempt was first made in (Heavens et al. 1998), and followed by various works (McDonald 2006; Matsubara 2008a; Jeong & Komatsu 2009; Saito et al. 2009; McDonald & Roy 2009; Manera et al. 2010; Baldauf et al. 2010a; Pollack et al. 2012; Sato & Matsubara 2011; Chan et al. 2012; Baldauf et al. 2012), which continuously show an improved understanding of the nonlinear galaxy power spectrum.

In this paper, we revisit the method of modeling the nonlinear power spectra of halos, more explicitly halo-matter and halo-halo power spectra, by incorporating the PT, the local bias model and the halo bias. In doing this, we employ “renormalization approach” developed in McDonald (2006) in order to re-sum contributions of the nonlinear matter clustering up to the higher-order loop corrections. This yields the term expressed by the product of the “full” nonlinear matter power spectrum and the renormalized linear bias parameter. The remaining terms, for which we keep the one-loop correction order based on the standard PT, give the effect of scale-dependent halo bias in the halo power spectrum. Thus our approach fully utilizes the recent improvement in modelling the nonlinear matter power spectrum (in this paper we will use the refined PT prediction developed in Taruya et al. (2009)). We test the accuracy of our model predictions by comparing with the halo spectra measured from high-resolution  $N$ -body simulations done in Nishimichi & Taruya (2011).

This paper is organized as follows. In Sec. 2, we develop a method of modeling the nonlinear halo-matter and halo-halo power spectra by incorporating the PT, the local bias model and the halo bias. In this section, we also show the detailed comparison of the model predictions with the simulation results for the halo catalogs of different mass bins. Throughout this paper we assume the  $\Lambda$  dominated, cold dark matter model ( $\Lambda$ CDM) as for our fiducial model which is consistent with Komatsu et al. (2011): the density parameters of matter, baryon and the cosmological constant are  $\Omega_{m0} = 0.279$ ,  $\Omega_{b0}/\Omega_{m0} = 0.165$ , and  $\Omega_{\Lambda} = 0.721$  (i.e. flat geometry), the Hubble parameter  $h = 0.701$ , the tilt of the primordial power spectrum  $n_s = 0.96$  and the power spectrum normalization  $\sigma_8 = 0.817$ .

## 2 PRELIMINARIES: PERTURBATION THEORY AND HALO BIAS

Our model is based on three ingredients; the perturbation theory (PT) of structure formation (Juszkiewicz 1981; Vishniac 1983; Fry 1984; Goroff et al. 1986; Suto & Sasaki 1991; Jain & Bertschinger 1994), the local bias model (Coles 1993; Fry & Gaztanaga 1993; Scherrer & Weinberg 1998) and the halo bias model (Mo & White 1996; Sheth & Tormen 1999) (also see Cooray & Sheth 2002; Bernardeau et al. 2002, for thorough reviews). In this section, we

briefly review the PT and the halo bias we will employ in the following sections.

### 2.1 Standard Perturbation Theory

Throughout this paper, we consider a pressure-less, irrotational fluid system and assume cold dark matter as the dominant fluid component to drive gravitational instability of structure formation. The nonlinear dynamics in an expanding universe is fully characterized by the density fluctuation field,  $\delta_m$ , and the peculiar velocity field  $\theta_m$  (Bernardeau et al. 2002). Given the initial conditions, the time evolutions of the fields are governed by the continuity equation, the equation of motion and the Poisson equation.

By using the standard PT, we can solve the nonlinear dynamics. The density fluctuation field at a given redshift  $z$  is expanded as

$$\delta_m(\mathbf{k}, z) = \delta_{m(1)}(\mathbf{k}, z) + \delta_{m(2)}(\mathbf{k}, z) + \delta_{m(3)}(\mathbf{k}, z) + \dots \quad (1)$$

The PT solution for the  $n$ -th order density fluctuation field can be found to be

$$\delta_{m(n)}(\mathbf{k}, z) \equiv D_+^n(z) \int d^3\mathbf{q}_1 \cdots d^3\mathbf{q}_n \delta_{m(1)}(\mathbf{q}_1) \cdots \delta_{m(1)}(\mathbf{q}_n) \times F_n(\mathbf{q}_1, \dots, \mathbf{q}_n) \delta_D^3\left(\mathbf{k} - \sum_i \mathbf{q}_i\right), \quad (2)$$

where  $\delta_{m(1)}$  is the linear density field today,  $D_+(z)$  is the linear growth rate normalized as  $D_+(z=0) = 1$ , and  $\delta_D^3(\mathbf{k})$  is the Dirac delta function. The  $n$ -th order density fluctuation field has the amplitude of the order  $O[(\delta_{m(1)})^n]$ . The growth rate can be computed, e.g. by solving Eq. (7) in Oguri & Takada (2011). The Fourier kernel  $F_n(\mathbf{q}_1, \dots, \mathbf{q}_n)$  describes a coupling between different Fourier modes due to nonlinear clustering, and we will use the expression in Eq. (10a) of Jain & Bertschinger (1994). Note that, although the form of the Fourier kernel is exact only for an Einstein de-Sitter model with  $\Omega_m = 1$ , it was shown to be a good approximation of the exact solution for a  $\Lambda$ CDM model.

### 2.2 Halo Mass Function and Halo Bias

Dark matter halos that host galaxies and/or galaxy clusters are useful tracers of large-scale structure, and can be used to infer the underlying dark matter distribution. However, the halo and dark matter distributions are not the same, which leaves an uncertainty, the so-called bias uncertainty. In this paper we employ the halo bias model developed in Mo & White (1996); Sheth & Tormen (1999) (also see Cooray & Sheth 2002).

Let us start with defining the halo mass function  $n(M, z)dM$ , which gives the comoving number density of halos in the mass range  $[M, M + dM]$  and at redshift  $z$ . We employ the mass function given in Sheth & Tormen (1999):

$$\begin{aligned} n(M)dM &= \frac{\bar{\rho}_{m0}}{M} f(v) dv \\ &= \frac{\bar{\rho}_{m0}}{M} A [1 + (av)^{-p}] \sqrt{av} \exp\left[-\frac{av}{2}\right] \frac{dv}{v}, \end{aligned} \quad (3)$$

where  $\bar{\rho}_{m0}$  is the mean mass density today;  $v \equiv [\delta_c/D_+(z)\sigma_m(M)]^2$ ;  $\delta_c$  is the threshold over-density for spherical collapse model;  $\sigma_m(M)$  is the present-day rms fluctuations in the mass density top-hat smoothed over scale  $R = (3M/4\pi\bar{\rho}_{m0})^{1/3}$ . We will throughout this paper employ the coefficients  $a = 0.75$  and  $p = 0.3$ , which

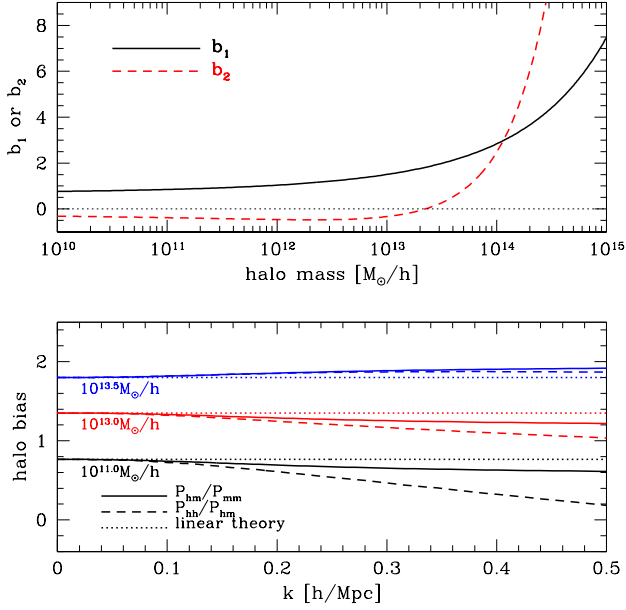


**Figure 1.** *Upper panel:* the halo bias parameters,  $b_1(M)$  and  $b_2(M)$ , as a function of halo mass, computed from Eq. (6). We consider  $\Lambda$ CDM model and redshift  $z = 0.35$ . The nonlinear bias parameter,  $b_2$ , is negative for low mass halos with  $M \lesssim 2.5 \times 10^{13}$ , while it becomes positive and rapidly increases for the more massive halos. *Lower panel:* the renormalized PT prediction for halo bias functions for halos with masses  $M = 10^{11}, 10^{13}$  and  $10^{13.5} M_\odot/h$  (from bottom to top curves), respectively. We used Eqs. (13) and (14) to compute these curves. Note that we set the effective bias parameter to  $b_1^{\text{eff}} = 0.9b_1(M)$  (0.9 times the linear halo bias parameter) as implied from the simulations (see Sec. 4), and set the residual shot noise term to  $\delta N = 0$  for simplicity.

are obtained by comparing the fitting formula to  $N$ -body simulations. Note that the normalization coefficient  $A$  is determined so as to satisfy the normalization condition  $\int_0^\infty dv f(v) = 1$ .

The mass function above holds only in an ensemble average sense, i.e. the average of the halo distribution over a sufficiently large volume. In other words, the number density of halos in a finite volume is modulated according to fluctuations of the underlying matter distribution within the volume,  $\delta_m$ . Employing the local bias model for halos, we assume that the halo distribution at a given spatial position  $\mathbf{x}$  is locally related to the underlying matter distribution at the position  $\mathbf{x}$  as

$$\begin{aligned} \delta_h(\mathbf{x}, z) &= F(\delta_m(\mathbf{x}, z)) \\ &= \sum_{n=0}^{\infty} \frac{1}{n!} F^{(n)}(\delta_m = 0) \{[\delta_m(\mathbf{x}, z)]^n - \langle [\delta_m(\mathbf{x}, z)]^n \rangle\}, \quad (4) \end{aligned}$$

where  $F$  is the functional to govern the local mapping relation. In the second line of the r.h.s., we have Taylor-expanded the relation in terms of  $\delta_m(\mathbf{x})$ , and  $F^{(n)}$  denotes the  $n$ -th derivatives of  $F$  with respect to  $\delta_m$ . Exactly speaking, as stressed in Schmidt et al. (2012), the local bias relation would hold to a good approximation in a “peak-background split” picture (also see Mo & White 1996; Sheth & Tormen 1999, for the pioneer work). In the peak-background model, the matter density field is divided into long- and short-wavelength modes, which correspond to “background” and “peak” density modes, respectively. The short-wavelength modes are at the scales responsible for formation of halos corresponding to about 10Mpc at maximum in the initial density fields and therefore are well below BAO scales (up to  $k \sim$  a few  $0.1 h/\text{Mpc}^{-1}$  in

wavenumber). The long-wavelength modes are a “coarse-grained” field responsible for a modulation of the peak heights of short-wavelengths, and in this paper we assume that the long-wavelength modes are at BAO scales. Hence we assume that  $\delta_m(\mathbf{x})$  in Eq. (4) is the coarse-grained field, even though we did not explicitly denote a notation to express the smoothing nature of  $\delta_m(\mathbf{x})$ . The term  $\langle [\delta_m(\mathbf{x})]^n \rangle$  in the above equation is introduced to enforce  $\langle \delta_h \rangle = 0$ .

As shown in Schmidt et al. (2012), the expansion coefficients in Eq. (4),  $F^{(n)}$ , can be related to the peak-background split bias parameters or halo bias parameters in an ensemble average sense. Since we focus on the halo correlation functions in this paper, we empirically assume that the halo density field in Fourier space is given as

$$\begin{aligned} \delta_h(\mathbf{k}, z) &= \sum_n \frac{b_n}{n!} \int d^3 \mathbf{q}_1 \cdots d^3 \mathbf{q}_n \delta_D^3 \left( \mathbf{k} - \sum_i \mathbf{q}_i \right) \\ &\quad \times \delta_m(\mathbf{q}_1, z) \cdots \delta_m(\mathbf{q}_n, z) + \epsilon(\mathbf{k}), \quad (5) \end{aligned}$$

where  $b_n$  is the halo bias parameters and we have set  $F^{(n)} = b_n$  when converting Eq. (4) to the above equation. The 1st and 2nd-order bias parameters, which are relevant for the results in the following sections, are given in terms of the derivatives of halo mass function (Eq. 3):

$$\begin{aligned} b_1(M) &= 1 + c_1 + E_1 \\ b_2(M) &= 2 \left( 1 - \frac{17}{21} \right) (c_1 + E_1) + c_2 + E_2, \quad (6) \end{aligned}$$

where

$$\begin{aligned} c_1 &= \frac{av - 1}{\delta_c}, \quad c_2 = \frac{av}{\delta_c^2} (av - 3), \\ E_1 &= \frac{2p/\delta_c}{1 + (av)^p}, \quad E_2 = \frac{1 + 2p}{\delta_c} + 2c_1. \quad (7) \end{aligned}$$

In Eq. (5), to keep more generality, we included the additional term  $\epsilon(\mathbf{k})$  to model the noise field that is uncorrelated to the matter density field, i.e.  $\langle \epsilon \delta_m \rangle = 0$  (see McDonald 2006). The term  $\langle [\delta_m(\mathbf{x})]^n \rangle$  in Eq. (4) contributes only to the monopole mode of  $k = 0$ , so we ignored the contribution as it is not relevant for the halo power spectra.

We again notice that Eq. (5) is not exact, and rather ansatz we employ in this paper. We will test how well our empirical, analytical model can describe the halo power spectra in the weakly nonlinear regime by comparing the model predictions with the simulation results.

### 3 RENORMALIZED PERTURBATION THEORY FOR NONLINEAR HALO POWER SPECTRA

In this section, we model nonlinear cross-power spectrum of matter and halos and nonlinear auto-power spectrum of halos by combining the “renormalized” PT approach (McDonald 2006; Saito et al. 2009; Jeong & Komatsu 2009; Saito et al. 2011) with the local bias model, the halo bias and the perturbation theory described in the preceding section.

#### 3.1 Halo-matter cross-power spectra

First, let’s consider the matter power spectrum defined as

$$\langle \delta_m(\mathbf{k}) \delta_m(\mathbf{k}') \rangle \equiv (2\pi)^3 P_m(k) \delta_D^3(\mathbf{k} + \mathbf{k}'). \quad (8)$$

Using Eq. (1), we can find that the power spectrum including up to the one-loop corrections are given as

$$P_m(k; z) = P_m^L(k; z) + P_{m(13)}(k; z) + P_{m(22)}(k, z), \quad (9)$$

where  $P_m^L(k; z)$  is the linear power spectrum, and  $P_{m(13)}$  and  $P_{m(22)}$  are the one-loop corrections arising from the ensemble averages of the higher-order matter density fluctuation fields;  $\langle \delta_{m(1)} \delta_{m(3)} \rangle$  and  $\langle \delta_{m(2)} \delta_{m(2)} \rangle$ , respectively. The one-loop corrections at a given redshift  $z$  can be computed once the linear power spectrum at the redshift is specified:

$$\begin{aligned} P_{m(13)} &\equiv \frac{k^3 P_m^L(k; z)}{252(2\pi)^2} \int_0^\infty dr P_m^L(kr; z) \left[ \frac{12}{r^2} - 158 + 100r^2 \right. \\ &\quad \left. - 42r^4 + \frac{3}{r^2}(r^2 - 1)^3(7r^2 + 2) \ln \left| \frac{1+r}{1-r} \right| \right], \\ P_{m(22)} &\equiv \frac{k^3}{98(2\pi)^2} \int_0^\infty dr P_m^L(kr; z) \\ &\quad \times \int_{-1}^1 d\mu P_m^L(k \sqrt{1+r^2-2r\mu}; z) \frac{(3r+7\mu-10r\mu^2)^2}{(1+r^2-2r\mu)^2}. \end{aligned} \quad (10)$$

Similarly, using the standard PT and halo bias prescription, we can compute the cross-power spectrum between matter and halos of mass  $M$ , which is the quantity that halo-shear cross-correlation can directly probe. By inserting Eq. (1) into Eq. (5), we can find the formal expression of the halo-matter cross-spectrum in a self-consistent manner by including up to the one-loop correction terms of  $\mathcal{O}(\delta_{m(1)}^4)$ :

$$\begin{aligned} P_{hm}(k; M, z) &= \left[ b_1 + \frac{\sigma^2}{2} \left( b_3 + \frac{68}{21} b_2 \right) \right] P_m^L(k) \\ &\quad + b_1 [P_{m(13)}(k) + P_{m(22)}(k)] \\ &\quad + b_2 \int \frac{d^3 \mathbf{q}}{(2\pi)^3} P_m^L(q) P_m^L(|\mathbf{k} - \mathbf{q}|) F_2(\mathbf{q}, \mathbf{k} - \mathbf{q}), \end{aligned} \quad (11)$$

where  $\sigma^2 \equiv \int d^3 \mathbf{q} / (2\pi)^3 P_m^L(q)$  and we employed notational simplification in the halo bias parameters;  $b_i = b_i(M)$ . Thus, a formal implementation of the standard perturbation theory (SPT)-based halo-matter spectrum yields the divergence term, i.e.  $\sigma^2 \sim \int^\infty q^3 P_m^L(q) d \ln q \rightarrow \infty$ , for a CDM-type power spectrum. In practice, since halo formation involves a coarse-grained smoothing of the underlying matter distribution corresponding to halo scales (also see discussion below Eq. 4), the divergence does not arise in the power spectrum we actually observe. Also note that the prefactor coefficient of the linear power spectrum  $P_m^L$  is independent of  $k$ .

From the first two terms of the r.h.s. of Eq. (11), we might re-write the two terms as

$$\begin{aligned} &\left[ b_1 + \frac{\sigma^2}{2} \left( b_3 + \frac{68}{21} b_2 \right) \right] P_m^L(k) + b_1 [P_{m(13)}(k) + P_{m(22)}(k)] \\ &= [b_1 + \delta b_1] P_m^L(k) + b_1 \delta P_m(k) \\ &\simeq [b_1 + \delta b_1] P_m^{\text{NL}}(k) + \mathcal{O}(\delta b_1 \delta P_m), \end{aligned} \quad (12)$$

where we have defined the notations  $\delta b_1 \equiv \sigma^2(b_3 + 68b_2/21)/2$  and  $\delta P_m \equiv P_{m(13)} + P_{m(22)}$ , which are the higher-order contributions to the linear bias and the linear matter power spectrum by the order of  $\mathcal{O}(\delta_{m(1)}^2)$  with respect to leading order in the PT formalism. Motivated by the equation above as well as the similar idea proposed by McDonald (2006), we propose the “renormalized” power spectrum as

$$\begin{aligned} P_{hm}(k; M, z) &\equiv b_1^{\text{eff}} P_m^{\text{NL}}(k; z) \\ &\quad + b_2(M) \int \frac{d^3 \mathbf{q}}{(2\pi)^3} P_m^L(q) P_m^L(|\mathbf{k} - \mathbf{q}|) F_2(\mathbf{q}, \mathbf{k} - \mathbf{q}). \end{aligned} \quad (13)$$

The first term is given by the nonlinear matter power spectrum,  $P_m^{\text{NL}}$ , multiplied by the “effective” or “renormalized” linear bias parameter,  $b_1^{\text{eff}}$ , while the second term includes the bare halo bias,  $b_2(M)$ , in Eq. (5). Thus the renormalized term can include the nonlinear corrections of matter clustering up to the higher orders. From the PT viewpoint, this is not self-consistent in a sense that the term  $b_1^{\text{eff}} P_m^{\text{NL}}$  includes the higher-order contributions than the one-loop order.

There are several nice features in our renormalization prescription:

- At the limit of small  $k$  or the linear regime,  $P_{hm}(k) \rightarrow b_1^{\text{eff}} P_m^L(k)$ , because  $P_m^{\text{NL}}(k) \rightarrow P_m^L(k)$  at the limit.
- The effective linear bias  $b_1^{\text{eff}}$  is a parameter, and is not related to the linear halo bias  $b_1(M)$  due to the renormalization. Observationally, however, it can be determined by the cross-power spectrum at small  $k$ , e.g. measured from the large-scale signal of galaxy-galaxy weak lensing (Mandelbaum et al. 2012).
- The scale-dependent bias, relative to the *nonlinear* mass power spectrum, arises from the term that depends on the second-order halo bias  $b_2(M)$  and the linear power spectrum. Therefore the term is predictable once the background cosmological model, the halo masses and the redshift are specified.

We will test an accuracy of the renormalized cross-power spectrum (Eq. 13) by comparing the predictions with simulation results for halos of various mass ranges. We will below show how the use of the “full” nonlinear matter power spectrum in Eq. (13) can give a better fit to the simulation.

### 3.2 Halo auto-power spectrum

Similarly, we propose the *renormalized* auto-power spectrum of halos with masses  $M$  and  $M'$  (for generality of discussion, we consider the case that halos are in different mass ranges):

$$\begin{aligned} P_{hh'}(k; M, M', z) &= \left[ b_1 b_1' + \frac{\sigma^2}{2} \left( b_1 b_3' + \frac{68}{21} b_1 b_2' \right) \right] \\ &\quad + \frac{\sigma^2}{2} \left( b_1' b_3 + \frac{68}{21} b_1' b_2 \right) \left[ P_m^L(k) + b_1 b_1' [P_{m(13)}(k) + P_{m(22)}(k)] \right] \\ &\quad + \frac{1}{2} b_2 b_2' \int \frac{d^3 \mathbf{q}}{(2\pi)^3} P_m^L(q) P_m^L(|\mathbf{k} - \mathbf{q}|) \\ &\quad + (b_1 b_2' + b_1' b_2) \int \frac{d^3 \mathbf{q}}{(2\pi)^3} P_m^L(q) P_m^L(|\mathbf{k} - \mathbf{q}|) F_2(\mathbf{q}, \mathbf{k} - \mathbf{q}) + \delta N \\ &\simeq b_1^{\text{eff}} b_1'^{\text{eff}} P_m^{\text{NL}}(k) \\ &\quad + \frac{1}{2} b_2 b_2' \int \frac{d^3 \mathbf{q}}{(2\pi)^3} \left[ P_m^L(q) P_m^L(|\mathbf{k} - \mathbf{q}|) - P_m^L(q)^2 \right] \\ &\quad + (b_1 b_2' + b_1' b_2) \int \frac{d^3 \mathbf{q}}{(2\pi)^3} P_m^L(q) P_m^L(|\mathbf{k} - \mathbf{q}|) F_2(\mathbf{q}, \mathbf{k} - \mathbf{q}) + \delta N', \end{aligned} \quad (14)$$

where we have introduced the effective linear bias  $b_1^{\text{eff}}$  and  $b_1'^{\text{eff}}$  for halos of masses  $M$  and  $M'$ , respectively, and used the collapsed notations such as  $b_2 = b_2(M)$  and  $b_2' = b_2(M')$  and similarly those for  $b_1$  and  $b_1'$ . The last term  $\delta N'$  denotes the residual shot noise term arising from  $\langle \epsilon(\mathbf{k}; M) \epsilon^*(\mathbf{k}'; M') \rangle$  in Eq. (5) as follows. As in the literature, we refer to the term as the residual noise component after subtracting the Poisson shot noise,  $1/n_h$ , without addressing the origin. Assuming that the residual shot noise is constant over the scale, but may vary with halo masses,  $\epsilon(\mathbf{k}, M) \rightarrow \epsilon(M)$ , we will below study whether the model including the residual shot noise can give a better fit to the  $N$ -body simulation results for halos of different mass



ranges. In the second line on the r.h.s. of the above equation, we redefined the shot noise term as  $\delta N' = \delta N + b_2 b_2' \int (d^3 \mathbf{q} / (2\pi)^3) P_m^L(q)^2$  so that the following term (the second term in the second line), which contributes to the scale-dependent bias, becomes finite for the limit  $k \rightarrow \infty$ :

$$\begin{aligned} & \frac{1}{2} b_2 b_2' \int \frac{d^3 \mathbf{q}}{(2\pi)^3} P_m^L(q) P_m^L(|\mathbf{k} - \mathbf{q}|) \\ & \rightarrow \frac{1}{2} b_2 b_2' \int \frac{d^3 \mathbf{q}}{(2\pi)^3} [P_m^L(q) P_m^L(|\mathbf{k} - \mathbf{q}|) - P_m^L(q)^2]. \end{aligned} \quad (15)$$

Since  $\int d^3 \mathbf{q} P_m^L(q)^2$  is constant, the residual shot noise term modified in this way is still constant in space, but can vary with halo masses both through the dependence on  $b_2(M) b_2(M')$  and  $\epsilon$ . The constant  $\delta N'$  needs to be treated as an additional free parameter for predicting  $P_{\text{hh}}(k)$ . In the following, we refer to the residual shot noise term as  $\delta N$ , instead of  $\delta N'$ , for notational simplicity. The effective bias parameter  $b_1^{\text{eff}}$  in Eq. (14) is the same to that in Eq. (13) up to the order  $\mathcal{O}(\delta_{m(1)}^2)$ .

We would like to notice features of the renormalized halo power spectrum:

- At the limit of small  $k$  or the linear regime,  $P_{\text{hh}}(k) \rightarrow b_1^{\text{eff}} b_1^{\text{eff}'} P_m^L(k) + \delta N$ .
- The scale-dependent bias depends on the linear power spectrum and the halo bias parameters,  $b_1(M)$  and  $b_2(M)$ , and therefore is predictable once the background cosmological model, the halo masses and the redshift are specified.
- The residual shot noise term  $\delta N$  needs to be included and treated as a free parameter.

It is worth mentioning difference between our approach and McDonald (2006). In McDonald (2006), all the bias coefficients are replaced with the renormalized bias parameters;  $b_1 \rightarrow b_1^{\text{eff}}$  and  $b_2 \rightarrow b_2^{\text{eff}}$ . Hence, the bias parameters need to be treated as free parameters, and their relations with the halo bias parameters were not discussed. We will below test the validity of Eq. (14) using simulations.

The lower panel of Fig. 1 shows the halo model predictions for the effective bias functions, which are defined in terms of the halo and matter power spectra:  $b^{\text{cross}}(k) \equiv P_{\text{hm}}(k)/P_m(k)$  or  $b^{\text{auto}}(k) \equiv P_{\text{hh}}(k)/P_{\text{hm}}(k)$  (see Eqs. 13 and 14). Note that we did not include the residual shot noise contribution in this plot (set  $\delta N = 0$ ). Our model predicts a scale dependent bias in the weakly nonlinear regime, and the degree of scale-dependence changes with halo masses. The top panel of Fig. 1 shows that  $b_2(M)$  is negative for low mass halos, goes to zero around  $M \approx 2 \times 10^{13} M_\odot/h$  and then becomes positive for more massive halos. Hence, Eqs. (13) and (14) tell that the nonlinear bias due to  $b_2(M)$  suppresses the power spectrum amplitudes for low mass halos, while it enhances for high mass halos. Also the model shows that, unlike the linear theory prediction, the scale-dependent halo bias generally differs in the estimators,  $P_{\text{hm}}/P_m$  and  $P_{\text{hh}}/P_{\text{hm}}$ . Hence  $r \neq 1$  in the weakly nonlinear regime, where  $r$  is the correlation coefficient of halo bias, defined as  $r \equiv P_{\text{hh}} / \sqrt{P_{\text{hm}} P_m}$ .

### 3.3 HOD model: Relating halos to galaxies

Although we have focused on the halo power spectra, halos are not a direct observable from a galaxy redshift survey and need to be inferred from the distribution of galaxies. A practically useful approach to relate galaxies to halos is using the halo occupation distribution (HOD) (Peacock & Smith 2000; Seljak 2000; Scoccimarro

et al. 2001). In this paper, for simplicity we assume that we can implement the method developed in Reid & Spergel (2009) (also see Reid et al. 2009, 2010; Hikage et al. 2012b,a) for reconstructing the halo distribution from the measured galaxy distribution. In the halo catalog, each halo hosts only one galaxy.

In this setting, there is only one galaxy per halo. The cross-power spectrum of matter and galaxies and the galaxy auto-power spectrum are given in terms of the halo spectra as

$$P_{gm}(k; z) = \frac{1}{\bar{n}_g} \int dM \frac{dn}{dM} N_{\text{HOD}}(M) P_{\text{hm}}(k; M, z), \quad (16)$$

$$\begin{aligned} P_{gg}(k; z) &= \frac{1}{\bar{n}_g^2} \int dM \frac{dn}{dM} N_{\text{HOD}}(M) \\ &\times \int dM' \frac{dn}{dM'} N_{\text{HOD}}(M') P_{\text{hh}}(k; M, M', z), \end{aligned} \quad (17)$$

where the spectra  $P_{\text{hm}}$  and  $P_{\text{hh}}$  are given by Eqs. (13) and (14), respectively. Here  $N_{\text{HOD}}(M)$  is the halo occupation distribution (HOD), and  $\bar{n}_g$  is the mean number density of galaxies, defined as  $\bar{n}_g \equiv \int dM (dn/dM) N_{\text{HOD}}(M)$ . Exactly speaking, the equations above are valid only if each galaxy is at the center of halo. When the galaxies have an offset from the halo center, we need to include a convolution of the average offset distribution of galaxies,  $\tilde{p}_{\text{off}}(k; M)$ , with the HOD distribution (see Hikage et al. (2012b,a) for details). However, for the real-space power spectrum we focus on in this paper, the effect is negligible on scales of interest;  $\tilde{p}_{\text{off}}(k; M) \approx 1$  at the scales of interest. For the redshift-space power spectrum, the off-centered galaxies cause a significant Fingers-of-God effect. The main focus of this paper is the scale-dependent galaxy bias due to nonlinearities of structure formation, so we focus on the real-space power spectrum.

Recently Hamaus et al. (2011) proposed a method, more directly based on the halo model approach, to model the nonlinear power spectrum of halos. In this method, the nonlinear halo-matter and halo-halo power spectra are given by a sum of the linear power spectrum, multiplied with linear bias parameter, and the 1-halo term. The 1-halo term of  $P_{\text{hm}}$  is calculated by the mass weighted integral of the mass function, because the Fourier-transformed halo profile  $\tilde{\rho}(k, M)/M \approx 1$  in the weakly nonlinear regime of interest. We will below compare the performance of our method and theirs by comparing the model predictions with our own high-resolution  $N$ -body simulations.

## 4 TESTING THE NONLINEAR HALO SPECTRA WITH $N$ -BODY SIMULATIONS

### 4.1 $N$ -body simulations and the halo catalogs

To test the accuracy of our method for modeling the halo-matter and halo-halo power spectra in the weakly nonlinear regime, we use  $N$ -body simulations for  $\Lambda$ CDM model done in Nishimichi & Taruya (2011). In brief, we adopted  $1280^3$   $N$ -body particles and the box size of volume  $1.5 (\text{Gpc}h^{-1})^3$ , and used the simulation outputs at  $z = 0.35$ . We defined halos using the Friends-of-Friends (FoF) finder algorithm with linking length 0.2 times the mean particle separation. For each halo, we use the total mass of member  $N$ -body particles as the halo mass, i.e. the FoF mass, and the center-of-mass positions of the particles as the halo position. Then we computed the halo power spectrum from the discrete distribution of halos in each simulation realization using the cloud-in-cells interpolation method and Fourier transformation. To reduce the statistical scatter, we use the mean spectra from 15 realizations. To explore the

Halo catalog	bin 1	bin 2	bin 3	bin 4	bin 5	bin 6	bin 7	bin 8	bin 9
$M_{\min}/10^{12} [M_{\odot}/h]$	1.55	2.18	3.11	4.37	6.22	8.77	12.5	17.6	24.9
$M_{\max}/10^{12} [M_{\odot}/h]$	4.86	8.95	15.3	23.3	35.4	59.3	104.4	182.5	–
$\bar{M}_h/10^{12} [M_{\odot}/h]$	2.60	4.08	6.21	8.22	12.9	19.1	28.2	40.6	61.7
$\bar{n}_h/10^{-4} [h^3\text{Mpc}^{-3}]$	15.7	12.6	9.46	6.87	4.87	3.47	2.43	1.64	1.09
$\bar{n}_h P_{\text{hh}}(k=0.1 \text{ hMpc}^{-1})$	7.35	6.78	5.90	4.97	4.16	3.57	3.06	2.52	2.12
$\bar{n}_h P_{\text{hh}}(k=0.2 \text{ hMpc}^{-1})$	2.71	2.54	2.22	1.88	1.58	1.34	1.14	0.93	0.76
$b_1^{\text{eff}}$ (from $P_{\text{hm}}/P_m$ )	1.06	1.13	1.22	1.32	1.44	1.60	1.78	1.99	2.27
$C$ (from SPT)	0.66	0.58	0.42	0.27	0.13	0.00	-0.14	-0.21	-0.29
$C$ (from CPT)	0.74	0.65	0.48	0.32	0.17	0.04	-0.10	-0.17	-0.24
$\bar{b}_1(M_h)$	1.17	1.25	1.34	1.44	1.55	1.69	1.91	2.10	2.33
$\bar{b}_2(M_h)$	-0.47	-0.45	-0.42	-0.36	-0.27	-0.12	0.22	0.60	1.19

**Table 1.** Summary of the catalogs of simulated halos, built from the  $N$ -body simulation outputs at  $z = 0.35$  for  $\Lambda$ CDM model (see text for details). We use the 9 halo catalogs, named as “bin 1”, ..., “bin 9”, which are different in their mass bins;  $M_{\min}$  and  $M_{\max}$  are the minimum and maximum masses to define each mass bin.  $\bar{M}_h$  and  $\bar{n}_h$  are the average halo virial masses and the mean number density of halos in each halo catalog, respectively. As an indicator of the shot noise contamination to the halo power spectrum, we give the values of  $\bar{n}_h P_{\text{hh}}$  at  $k = 0.1$  and  $0.2 \text{ hMpc}^{-1}$ , respectively, measured from the simulations. The quantity  $b_1^{\text{eff}}$  is the renormalized linear bias parameter, which is estimated by comparing the PT model prediction to the simulation result for the halo-matter spectrum,  $P_{\text{hm}}(k)$ , at large scales ( $k < 0.05 \text{ hMpc}^{-1}$ ) for each halo catalog (see text for details). The quantity  $C$  is the best-fit parameter to characterize the residual shot noise, estimated by fitting the PT model to the simulation result for the halo power spectrum,  $P_{\text{hh}}(k)$ , in the weakly nonlinear regime (see text). The values  $\bar{b}_1(M_h)$  and  $\bar{b}_2(M_h)$  are the halo bias parameters averaged by the halo mass function over the halo mass range. The effective bias parameter  $b_1^{\text{eff}}$  differs from the halo bias  $\bar{b}_1(M_h)$  by about 10% for the halo masses we consider.

validity of our model for different ranges of halo masses, we divided the halos into different mass bins. Table 1 shows the parameters of the halo catalogs; we consider the halo catalogs divided into 9 mass bins, with mean masses ranging from  $2.96 \times 10^{12}$  to  $7.03 \times 10^{13} M_{\odot}/h$ . Note that, for the following results, we use the shot-noise-subtracted halo spectra, where we subtracted the theory-expectation  $1/\bar{n}_h$  from the halo spectra measured from the simulations ( $\bar{n}_h$  is the mean number density of halos in a given simulation).

The halo bias and the halo mass function we use are given as a function of the virial mass, rather than the FoF mass. We use the conversion relation  $M_{\text{vir}} = 0.88 M_{\text{FoF}}$  at  $z = 0.35$  to estimate the average virial mass for each mass bin using the method in Hu & Kravtsov (2003), where we assume that the FoF halo mass is close to the enclosed mass  $M_{180b}$  (White 2002) inside which the mean density is 180 times the mean mass density and also assume that each halo follows an Navarro-Frenk-White profile (Navarro et al. 1997) with concentration parameter  $c_{\text{vir}} = 4$ . We should note that this mass conversion only slightly changes the model predictions for the halo spectra, by up to a few % in the amplitudes.

To compute the power spectrum for halos in the finite mass range used for the halo catalogs in Table 1, we use the following HOD in our model (Eqs. 16 and 17):

$$N_{\text{HOD}}(M) = \begin{cases} 1 & \text{if } M_{\min,i} \leq M \leq M_{\max,i}, \\ 0 & \text{otherwise.} \end{cases} \quad (18)$$

## 4.2 Halo-matter cross-power spectrum

First, we study the halo-matter cross-power spectrum and define the bias function, for convenience of the following discussion, as

$$b_{h_i}^{\text{cross}}(k) \equiv \frac{P_{h_i,m}(k)}{P_m(k)}, \quad (19)$$

where  $P_{h_i,m}$  is the cross-spectra between dark matter ( $N$ -body) particles and halos of the  $i$ -th mass bin, and  $P_m$  is the matter power spectrum computed from the original  $N$ -body simulations. The shot noise is negligible for the cross-spectrum  $P_{h_i,m}$ .

The data points in Fig. 2 show the bias function  $b_{h_i}^{\text{cross}}(k)$  mea-

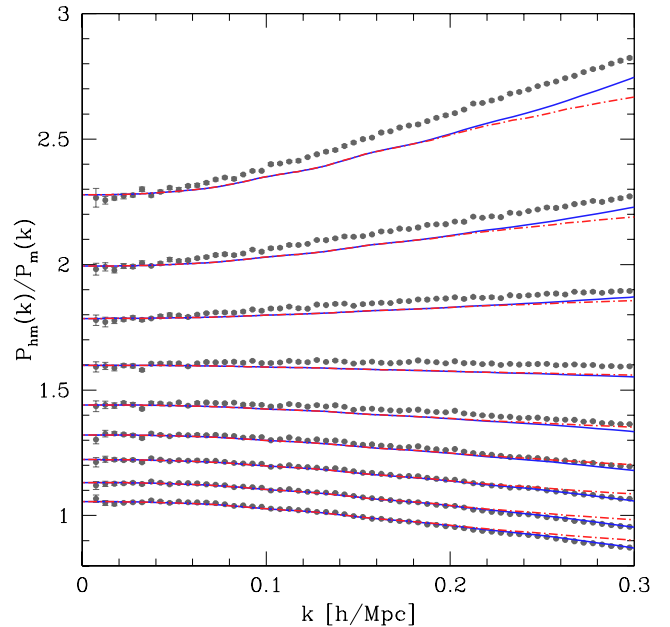


**Figure 2.** The bias function  $b_h^{\text{cross}}(k)$ , defined as  $b_h^{\text{cross}}(k) \equiv P_{\text{hm}}(k)/P_m(k)$  for halos of different mass ranges given in Table 1. The symbols are the simulation results, which are computed from 15 simulation realizations (see text for details), and clearly show a scale-dependent bias at  $k \gtrsim 0.1 \text{ hMpc}^{-1}$ . The red dot-dashed curves show the PT predictions including up to the one-loop correction (Eqs. 13 and 16). We determined the free parameter of the model prediction, the effective linear bias parameter  $b_1^{\text{eff}}$ , by fitting the model prediction to the simulation result up to  $k \leq 0.05 \text{ hMpc}^{-1}$  for each halo mass bin. The scale-dependent bias is from a combination of the halo bias ( $b_2$ ) and the nonlinear matter power spectrum. The solid curves show the model predictions when using the improved PT model prediction given in Nishimichi & Taruya (2011) for the nonlinear matter power spectrum  $P_m^{\text{NL}}$  instead of the standard PT.

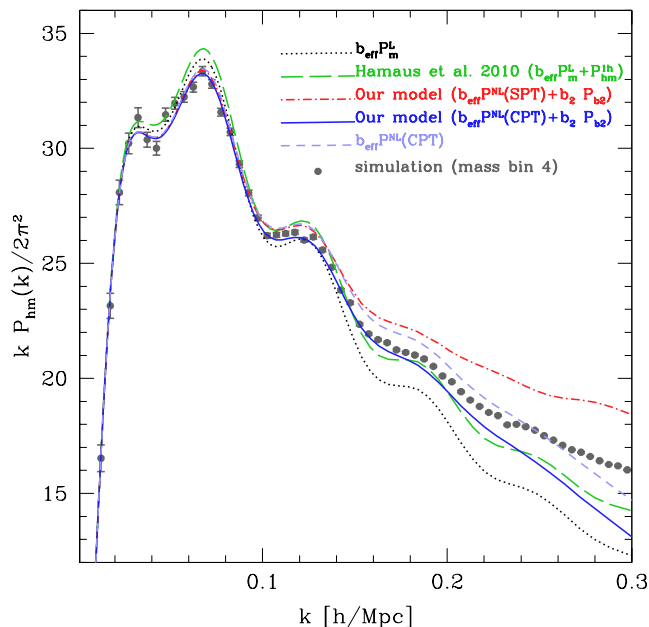


**Figure 3.** The halo-matter cross-power spectrum  $P_{hm}(k)$  for halos of mass bin “4” (Table 1), plotted in the unit of  $kP_{hm}(k)/2\pi^2$  so that the features in the weakly nonlinear regime including the BAO features become prominent. The symbols are the simulation result as in Fig. 2, while the error bars are the statistical uncertainties at each  $k$  bins estimated from the 15 realizations. The dotted-dashed curve denotes the model prediction (Eq. 13) obtained by using the standard PT to compute the nonlinear matter power spectrum  $P_m(k)$  including up to one-loop corrections. The solid curve is the result if using the improved PT prediction (CPT) for  $P_m(k)$ , which shows an improved agreement with the simulation result up to the higher  $k$ . To see the effect of scale-dependence bias arising from  $b_2$ , the short dashed curve shows  $b_1^{\text{eff}} P_m^{\text{CPT}}(k)$ , i.e. the nonlinear matter power spectrum (CPT) multiplied by the effective linear bias parameter. The dotted curve is the linear theory prediction,  $b_1^{\text{eff}} P_m^{\text{L}}(k)$ . For comparison, we also show the model prediction recently proposed in Hamaus et al. (2011), which models the halo-matter power spectrum fully based on the halo model: the linear theory plus the 1-halo term given as  $b_1^{\text{eff}} P_m^{\text{L}}(k) + P^{1h}(k)$ .

sured from the simulations. The spectra  $P_{hm}$  and  $P_m$  in each simulation share the same large-scale structure, and therefore the scatters due to the sampling variance mostly cancel in the ratio, yielding relatively smoothly-varying data points over  $k$ . The figure clearly shows that the halo bias has greater amplitudes for more massive halos. At sufficiently large scales or small  $k$ ,  $k \lesssim 0.08 \text{ hMpc}^{-1}$ , the halo bias appears to be constant, implying that the linear bias model is valid at the large scales. On the other hand, at the larger  $k$ , the simulation results manifest a scale-dependent halo bias for all the halo mass bins.

The dot-dashed curves show our model predictions computed using Eq. (13). To compute the model predictions, we need to fix one free parameter, the renormalized linear bias  $b_1^{\text{eff}}$ , for which we determined  $b_1^{\text{eff}}$  by fitting the model-predicted  $b^{\text{cross}}(k)$  to the simulation  $b^{\text{cross}}(k)$  in the linear regime, at  $k \leq 0.05 \text{ hMpc}^{-1}$ . Table 1 shows that the best-fit  $b_1^{\text{eff}}$  differs from the linear halo bias by about 10%, which is also found by Manera et al. (2010). In our method, we interpret that the discrepancy between  $b_1$  and  $b_1^{\text{eff}}$  arises due to the renormalization;  $b_1^{\text{eff}}$  has a contribution of the higher-order moments (see around Eq. 12) in addition to  $b_1$ . However, the discrepancy might also be ascribed partly to the inaccuracy of the analytical halo mass function (Eq. 3), compared with our  $N$ -body simula-

tions, as well as to violation of the universality of the mass function. (e.g. Tinker et al. 2008). However, exploring these issues is beyond the scope of this paper, so we leave these for future work. Besides this free parameter, we used the input  $\Lambda$ CDM model parameters and halo mass range to compute the model prediction. Once the parameter  $b_1^{\text{eff}}$  is determined, our model can be in remarkably good agreement with the simulation results, including the  $k$ -dependence and the halo mass-dependence. For the largest mass bin, our model shows a sizable disagreement, possibly due to an inaccuracy of the halo mass function used for the model calculation or the breakdown of perturbation theory to describe too strong nonlinear bias.

At large  $k$ , the perturbation theory ceases to be accurate, and is indeed not accurate enough up to  $k \sim 0.2 \text{ hMpc}^{-1}$ . There have been many efforts to improve the PT prediction of nonlinear matter power spectrum by including the higher-order loop corrections, e.g. the renormalized PT (Crocco & Scoccimarro 2006; Taruya et al. 2009, also see references therein). The solid curve shows the results if we use the improved PT prediction for the nonlinear matter power spectrum  $P_m^{\text{NL}}$  that is taken from Nishimichi & Taruya (2011) (also see Taruya et al. 2009) (the closure theory; hereafter CPT), instead of the standard PT including up to the one-loop correction. The improved  $P_m^{\text{NL}}$  has smaller amplitudes in the weakly nonlinear regime  $k \gtrsim 0.1 \text{ hMpc}^{-1}$  at the redshift  $z = 0.35$  than the standard PT predicts, yielding a slightly stronger scale-dependence of  $b(k)(= P_{hm}/P_m^{\text{NL}})$  as evident from Eq. (13). The improved  $P_m^{\text{NL}}$  shows a similar-level agreement with the simulation results.

In order to see the accuracy of our model for  $P_{hm}(k)$ , we compare the simulation result for  $P_{hm}$  with the different model predictions in Fig. 3. Here we considered the intermediate halo mass bin (bin 4), and we use the parameter  $b_1^{\text{eff}}$  determined in Fig. 1. Encouragingly, the figure clearly shows that our model prediction well agrees with the simulation  $P_{hm}(k)$  up to  $k \approx 0.2 \text{ hMpc}^{-1}$ , if we use the improved PT model (CPT) for the nonlinear matter power spectrum. If we use the standard PT theory instead, the agreement is only up to  $k \approx 0.12 \text{ hMpc}^{-1}$ , and the standard PT breaks down at the larger  $k$ , in the weakly nonlinear regime. Hence we conclude that the apparent agreement of the standard PT up to the higher  $k$  bins in Fig. 1 is due to a cancellation of inaccuracies in the two spectra  $P_{hm}$  and  $P_m$ , in the numerator and denominator of the bias function  $b^{\text{cross}}(k)$ . Comparing the solid and short-dashed curves shows the effect of nonlinear scale-dependent bias that arises from the term proportional to  $b_2(M)$  in Eq. (13). The scale-dependent bias becomes important at  $k \gtrsim 0.1 \text{ hMpc}^{-1}$  for this redshift  $z = 0.35$ , and our model can reproduce the simulation result.

The dashed curve shows the model prediction recently proposed in Hamaus et al. (2011), where the nonlinear power spectrum is computed based on the halo model in combination with the halo bias parameters. The figure shows that the agreement is not as good as our model prediction.

### 4.3 Halo auto-power spectrum

The model parameters for the halo power spectrum  $P_{hh}(k)$  are  $b_1^{\text{eff}}$  and the residual shot noise parameter  $\delta N$ . For convenience of our discussion, we use the following parametrization of the residual shot noise term relative to the standard shot noise term:

$$\delta N_{hi} = C_i \frac{1}{\bar{n}_{hi}}. \quad (20)$$

Fig. 4 compares the PT predictions and the simulation results for  $P_{hh}(k)$ , as in Fig. 3. To compute the PT predictions, we determined the free parameters  $b_1^{\text{eff}}$  and  $C$  for each halo catalog

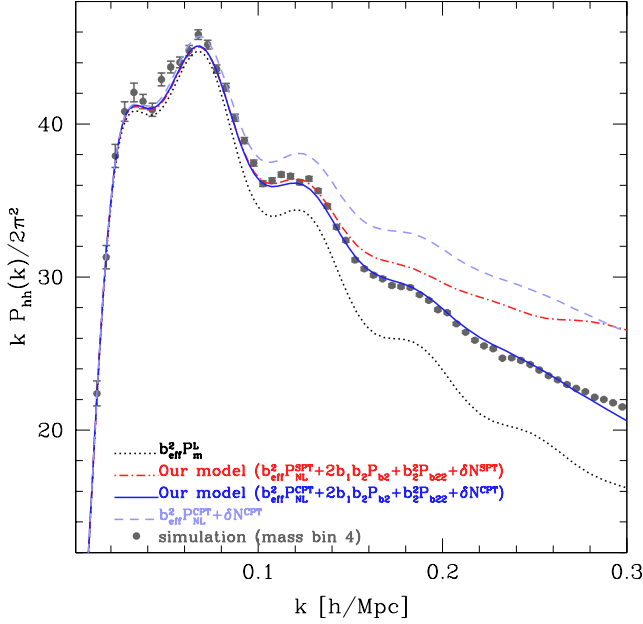


**Figure 4.** As in Fig. 3, but for the halo auto-power spectrum  $P_{hh}(k)$ . The symbols show the simulation result for the halo catalog of mass bin 4, where the standard shot noise term  $1/\bar{n}_h$  is subtracted from the measured power spectrum. The dot-dashed and solid curves are the model predictions (Eq. 14), where we used the standard PT and the improved PT (CPT) to compute the nonlinear matter power spectrum  $P_m^{\text{NL}}(k)$ , respectively. To compute the model predictions, we used the same linear bias parameter  $b_1^{\text{eff}}$  in Fig. 2, and determined the residual shot noise parameter  $\delta N$  from the fitting of each model prediction to the simulation result up to  $k = 0.2 \text{ hMpc}^{-1}$ . To illuminate the scale-dependent bias, the dashed curve shows the model prediction ignoring the terms of halo bias parameters in Eq. (14); i.e.  $(b_1^{\text{eff}})^2 P_m^{\text{CPT}}(k) + \delta N$ . The dotted curve is the linear theory prediction,  $(b_1^{\text{eff}})^2 P_m^{\text{L}}$ .

as follows. For  $b_1^{\text{eff}}$ , we used the same values as those used for the halo-matter cross-power spectra in Fig. 2. For  $C$ , we determined the value by fitting the model prediction to the simulation result up to  $k_{\text{max}} = 0.15$  or  $0.20 \text{ hMpc}^{-1}$  for the SPT or the improved PT (CPT), respectively. The maximum wavenumber  $k_{\text{max}}$  is chosen because each of the PT models for nonlinear matter power spectrum is accurate enough up to the  $k_{\text{max}}$ -wavenumber to within about 3% accuracy (Nishimichi & Taruya 2011). In doing this fitting, we accounted for the statistical uncertainties in estimating the power spectrum from the 15 simulation realizations; i.e., we used the weighting in each  $k$ -bin, given as  $(\Delta P_{hh})^2 \propto 1/(2\pi k_i^2 \Delta k)[P_{hh}(k_i) + 1/\bar{n}_h]^2$  ( $k_i$  is the central value of the  $i$ -th  $k$ -bin and  $\Delta k$  is the width). The best-fit residual shot noise parameter  $C$  is about 30% compared to the standard shot noise for this halo mass bin (bin 4). Table 1 shows a strong anti-correlation between  $C$  and halo mass. The anti-correlation might be ascribed to a mass dependence of the stochastic halo bias (Matsubara 1999; Taruya & Suto 2000).

As can be found from Fig. 4, our model prediction is in good agreement with the simulation result, apparently up to  $k \approx 0.25 \text{ hMpc}^{-1}$ , if we use the improved PT prediction (solid curve)<sup>4</sup>.

<sup>4</sup> Note that, exactly speaking, the improve PT (CPT) ceases to be accurate at  $k > 0.2 \text{ hMpc}^{-1}$ , so the apparent agreement at the scales is as a result of the residual shot noise contribution, which happens to match the simulation result.

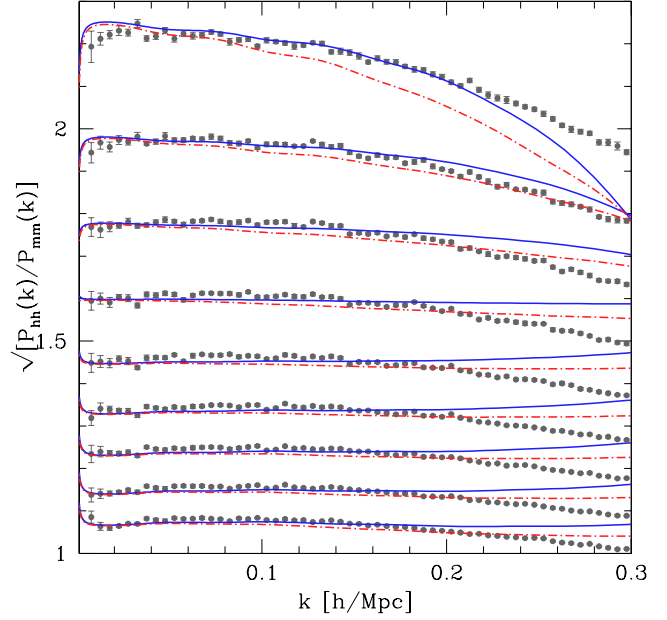


**Figure 5.** The bias function defined in terms of the halo auto-spectrum as  $b_{hi}^{\text{auto}}(k) = \sqrt{P_{hh}(k)/P_m(k)}$  for each halo mass as in Fig. 2. The linear theory predicts no scale dependence and that the bias amplitude is the same to that of large scale limit for  $P_{hm}(k)/P_m(k)$  in Fig. 2. The symbols are the simulation results for different halo masses, where the standard shot noise  $1/\bar{n}_h$  is subtracted. To compute the model predictions, we need to fix the free parameters: we used the same  $b_1^{\text{eff}}$  to that in Fig. 2 and determined the residual shot noise parameter  $C$  by fitting the model prediction to the simulation result up to  $k \leq 0.2 \text{ hMpc}^{-1}$ .

The nice agreement is found by including the residual shot noise contribution, which can account for a part of the nonlinear bias effect. The standard perturbation theory cannot achieve the similar level agreement, even if varying the residual shot noise parameter. The figure also shows other model predictions, and the comparison of different model predictions manifests the importance of nonlinear clustering effect and scale-dependent bias in the weakly nonlinear regime. Combining the results in Figs. 3 and 4 implies that the halo bias parameters  $b_1(M)$  and  $b_2(M)$ , in combination with the nonlinear matter power spectrum and the residual shot noise, can well reproduce the halo spectra  $P_{hm}(k)$  and  $P_{hh}(k)$ .

Now we study another bias function defined in terms of the halo power spectrum as

$$b_{hi}^{\text{auto}}(k) \equiv \sqrt{\frac{P_{hi} b_{hi}(k)}{P_m(k)}}. \quad (21)$$

This bias function is different from the bias function  $b^{\text{cross}}(k)$  we studied in Fig. 1, as can be explicitly found from Eqs. (13) and (14) (also Eqs. 16 and 17). Fig. 5 compares the PT predictions and the simulation results for the bias function of each halo catalog  $b_{hi}^{\text{auto}}(k)$ , where the PT predictions are computed by using the best-fit power spectra  $P_{hm}$  and  $P_{hh}$  as estimated in Figs. 2 and 4. Note that the model in Fig. 5 appears to show a larger disagreement with the simulation result at  $k > 0.2 \text{ hMpc}^{-1}$ , compared to Fig. 4, especially when using the CPT for  $P_m^{\text{NL}}$ . This is mainly because of the unphysical damping of the CPT model for the  $P_m^{\text{NL}}$  at that scales (Taruya et al. 2009), and partly because the plotting range of  $y$ -axis in Fig. 5 is narrower than in Fig. 4. We should notice that the discrepancy of the model from the simulation is less than 1% at  $k < 0.2 \text{ hMpc}^{-1}$  for both the plots. The best-fit value of the residual shot noise pa-



parameter,  $C$ , for each halo mass bin is given in Table 1. The amount of the residual shot noise varies with halo masses, ranging from a few % to 70% compared to the standard shot noise term, and changes from negative to positive values from less to more massive halos. The bias function  $b^{\text{auto}}(k)$  shows a scale-dependence over the range of  $k$  we consider. The scale-dependence of  $b^{\text{auto}}$  indeed differs from that of  $b^{\text{cross}}(k)$  in Fig. 2 as the PT model predicts. The model predictions can fairly well reproduce the simulation results up to  $k \approx 0.2 h\text{Mpc}^{-1}$ , but then show a larger disagreement at the larger  $k$  than in Fig. 2 due to inaccuracies in both the model predictions for  $P_{\text{hm}}$  and  $P_{\text{hh}}$ .

#### 4.4 Comparison of halo bias model with other models

The main difference between our method and the previous works (McDonald 2006; Jeong & Komatsu 2009; Saito et al. 2009; Baldauf et al. 2010a; Saito et al. 2011), is whether or not to incorporate the renormalized bias approach and the halo bias into the PT approach for computing the nonlinear power spectra. In this section, we compare our model predictions with other models that have similar forms.

The nonlinear power spectra in these models are expressed by the following general forms (see Eqs. 13 and 14 for our model):

$$\begin{aligned} P_{\text{hm}}(k) &= \alpha_1 P_m^{\text{NL}}(k) + \alpha_2 P_{b_2}(k), \\ P_{\text{hh}}(k) &= \alpha_1^2 P_m^{\text{NL}}(k) + 2\alpha_3 P_{b_2}(k) + \alpha_2^2 P_{b,22} + \alpha_4, \end{aligned} \quad (22)$$

where

$$\begin{aligned} P_{b_2}(k) &\equiv \int \frac{d^3 \mathbf{q}}{(2\pi)^3} P_m(q) P_m(|\mathbf{k} - \mathbf{q}|) F_2(\mathbf{q}, \mathbf{k} - \mathbf{q}), \\ P_{b,22}(k) &\equiv \frac{1}{2} \int \frac{d^3 \mathbf{q}}{(2\pi)^3} [P_m(q) P_m(|\mathbf{k} - \mathbf{q}|) - P_m(q)^2]. \end{aligned} \quad (23)$$

In terms of these forms, we can categorize the different models as

- *Our model*:  $\alpha_1 = b_1^{\text{eff}}$ ,  $\alpha_2 = b_2(M)$ ,  $\alpha_3 = b_1(M)b_2(M)$ ,  $\alpha_4 = \delta N$ , where  $b_1(M)$  and  $b_2(M)$  are the halo bias parameters and  $b_1^{\text{eff}}$  and  $\delta N$  are treated as free parameters.
- *Saito et al. 2009*: This is based on a renormalized perturbation theory originally proposed in McDonald (2006). Here the coefficients are set to  $\alpha_1 = b_1$ ,  $\alpha_2 = b_2$ ,  $\alpha_3 = b_1 b_2$ , and  $\alpha_4 = \delta N$ , and the three ( $b_1$ ,  $b_2$ ,  $\delta N$ ) are treated as free parameters to be determined by the fitting. This method is also studied in Baldauf et al. (2010b).
- *McDonald 2006*: This is similar to the method ‘‘Saito et al. 2009’’, but uses the nonlinear matter power spectra  $P_m^{\text{NL}}$  for  $P_m$ ’s in  $P_{b_2}$  and  $P_{b,22}$ , instead of the linear spectrum. This method is intended to include renormalization for bias parameters as well as for the nonlinear matter power spectrum.
- *4 free parameters*: This is a variant of our model. The coefficients are set to  $\alpha_1 = b_1^{\text{eff}}$ ,  $\alpha_2 = b_2$ ,  $\alpha_3 = b_1 b_2$ ,  $\alpha_4 = \delta N$ , and all the 4 parameters ( $b_1^{\text{eff}}$ ,  $b_1$ ,  $b_2$ ,  $\delta N$ ) are treated as free parameters.

Note that, to have a fair comparison, we use CPT to compute  $P_m^{\text{NL}}(k)$  in the first term of Eq. (22) for all the above models. Thus the different models have different ranges of their variations in the power spectra as a function of  $k$  with varying free parameters for a given cosmological model.

Fig. 6 shows the different model predictions, described above, for  $P_{\text{hm}}$  and  $P_{\text{hh}}$  for different halo mass bins, compared to the simulation results. To determine the free parameters in each model, we minimize the following  $\chi^2$  by comparing the model prediction to the simulation result:

$$\chi^2 = \sum (\mathbf{P}^{\text{sim}} - \mathbf{P}^{\text{model}})^T \mathbf{C}^{-1} (\mathbf{P}^{\text{sim}} - \mathbf{P}^{\text{model}}), \quad (24)$$

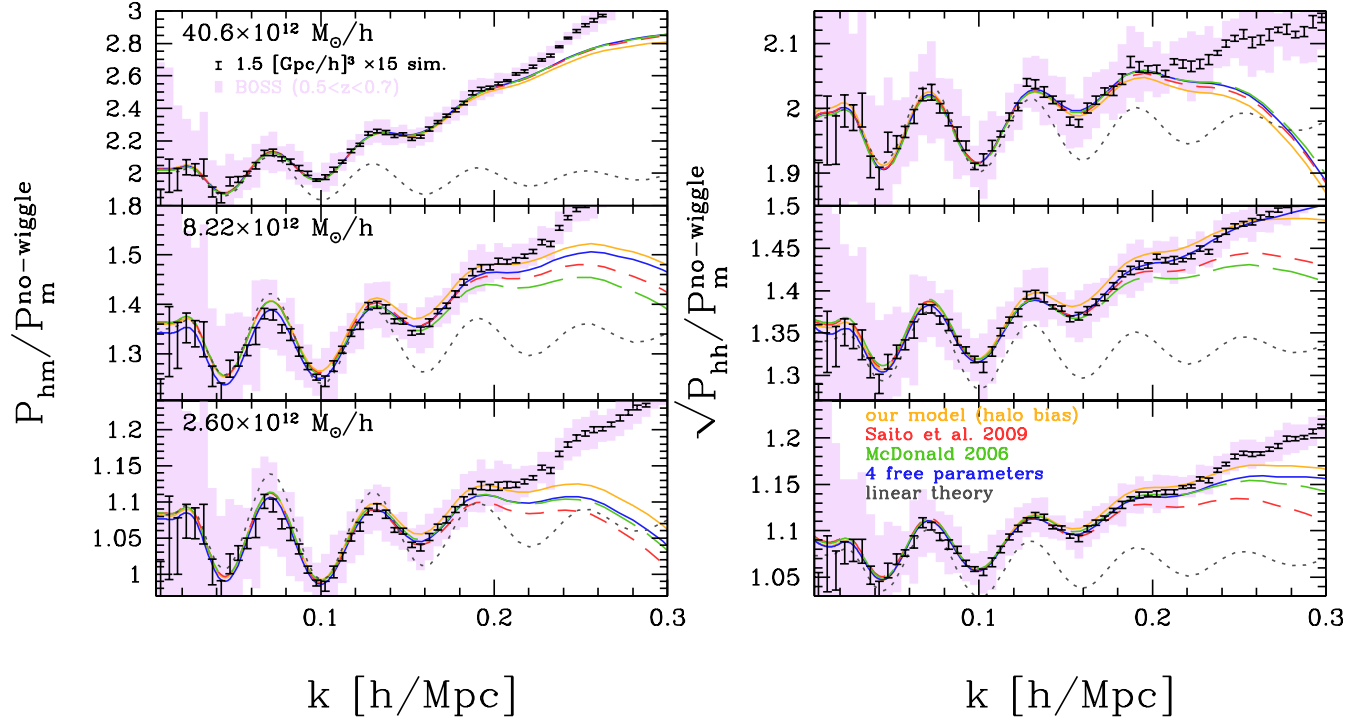
where  $\mathbf{P}(k_i) = [P_{\text{hm}}(k_i), P_{\text{hh}}(k_i)]$ , the power spectra with superscripts ‘‘sim’’ or ‘‘model’’ are the simulated or model power spectra, respectively,  $\mathbf{C}$  is the covariance matrix of the power spectrum computed from 15 realizations of the simulated power spectra, and  $\mathbf{C}^{-1}$  is the inverse matrix. We use the power spectrum information up to  $k_{\text{max}} = 0.2 h\text{Mpc}^{-1}$ . We included correlation between  $P_{\text{hm}}$  and  $P_{\text{hh}}$  at the same  $k$ -bin in the covariance matrix, but ignored correlations between different  $k$  bins for simplicity<sup>5</sup>. Our choice of  $k_{\text{max}} = 0.2 h\text{Mpc}^{-1}$  is based on the fact that the CPT prediction for  $P_m^{\text{NL}}(k)$  is accurate to within a 3% level up to  $k = 0.2 h\text{Mpc}^{-1}$  compared to the simulated spectrum at  $z = 0.35$  as shown in Nishimichi & Taruya (2011).

Fig. 6 shows that the different models well reproduce the simulated  $P_{\text{hm}}$  or  $P_{\text{hh}}$  to an equal-level accuracy up to  $k \approx 0.15$  or  $0.2 h\text{Mpc}^{-1}$  in some cases. Again note that our model has least free parameters among these models, because our model uses the halo bias parameters  $b_1(M)$  and  $b_2(M)$  to model the scale-dependent bias of the nonlinear halo power spectra (Eqs. 22), and therefore restricts a range of the model variations compared to other models. Nevertheless, our model appears to be reasonably accurate compared to other models.

For comparison, the shaded region around the curves in Fig. 6 shows  $1\sigma$  statistical errors of the power spectrum measurements expected for a survey with volume coverage of about  $3.4 (\text{Gpc}h^{-1})^3$ , which roughly corresponds to the volume of a BOSS-like survey with redshift range  $0.5 \leq z \leq 0.7$  and area coverage 10,000 square degrees. We estimated the error bars by scaling the scatters at each  $k$  bin from the 15 simulation realizations assuming that the scatters scale with a survey volume as  $\sigma(P) \propto 1/\sqrt{V_s}$ . It can be found that our model is accurate at least enough up to  $k \approx 0.20 h\text{Mpc}^{-1}$  within the  $1\sigma$  errors for a BOSS-like survey, for a different range of halo masses. The linear theory is not accurate at BAO scales, at  $k \gtrsim 0.1 h\text{Mpc}^{-1}$ , although the PT based model also ceases to be accurate at  $k \gtrsim 0.2 h\text{Mpc}^{-1}$ .

Fig. 7 and Table 2 give a more quantitative comparison of our model with other models, where we consider the BOSS-like survey to compute the  $\chi^2$  given the expected measurement accuracies as in Fig. 6. Fig. 7 compares the best-fit coefficients ( $\alpha_1, \dots, \alpha_4$ ), which can be read as effective bias parameters (see below Eq. 22), with the results of our model; the halo bias parameters ( $b_1(M), b_2(M)$ ) and the best-fit parameters  $b_1^{\text{eff}}$  and  $\delta N$ . The figure shows that the results for ‘‘Saito et al. (2009)’’ or ‘‘McDonald 2006’’ reproduce the similar results to our model. The model ‘‘4 free parameters’’ shows a sizable difference from our result, especially for  $\alpha_3$  and  $\delta N$ , implying that even small changes in the coefficients give the similar nonlinear power spectra for  $P_{\text{hm}}^{\text{NL}}$  and  $P_{\text{hh}}$  at the scales. This also means a strong degeneracy between  $\alpha_3$  and  $\delta N$  parameters. Table 2 gives the reduced  $\chi^2$  of the best-fit model power spectra for each model and for each halo mass bin. Here we consider  $k_{\text{max}} = 0.15$  or  $0.2 h\text{Mpc}^{-1}$  for the maximum wavenumber to use for the model fitting. The degrees of freedom are defined by the number data point of the simulated spectra (58 or 78 in total for  $P_{\text{hm}}$  and  $P_{\text{hh}}$  when employing  $k_{\text{max}} = 0.15$  or  $0.2 h\text{Mpc}^{-1}$ , respectively) minus the number of free parameters (either 2, 3 or 4). Again our model and the models ‘‘Saito et al. (2009)’’ or ‘‘McDonald (2006)’’ are in a similar-level accuracy, and the model ‘‘4 free parameters’’ is

<sup>5</sup> This assumption would not cause any serious systematic errors as the scales we consider are in the weakly nonlinear regime and the non-Gaussian errors, which cause correlations between different  $k$  bins, are not significant as studied in Takahashi et al. (2009).



**Figure 6.** Comparison of the different PT-based model predictions for the halo-matter cross-power spectrum (*left panel*) and the halo auto-power spectrum (*right panel*), for the three halo catalogs of different mass bins (the 1, 4 and 8 mass bins in Table 1). For illustrative purpose, the power spectra are normalized by the nonlinear matter power spectrum without BAO wiggles. For comparison, the dotted curves are the linear theory prediction (the power spectra in the denominator and numerator are both the linear power spectra). The different models are expressed by the similar forms (Eq. 22), and have a different number of free parameters (2, 3 and 4 parameters), as indicated by legends and explained below Eq. (22). The data with error bars at each  $k$ -bin are the spectra estimated from 15 realizations each of which has a  $1.5 (\text{Gpc}h^{-1})^3$  volume, and the error bar is the  $1\sigma$  scatter of the central value at each  $k$ -bin, which is estimated by dividing the scatters of 15 realizations by  $\sqrt{15}$ ; i.e.  $1\sigma$  statistical scatter for a volume of  $15 \times 1.5 (\text{Gpc}h^{-1})^3$ . The best-fit parameters for each model are obtained by comparing the model predictions to the simulation taking into account the statistical errors (Eq. 24). The shaded region at each  $k$  bin is the errors expected for a BOSS-like survey of  $3.4 (\text{Gpc}h^{-1})^3$  volume, obtained by assuming that the error bars scales with survey volume ( $V_s$ ) as  $\sigma(P) \propto 1/\sqrt{V_s}$ . Our model and the other models show a similar-level agreement with the simulations, to within the  $1\sigma$  error bars of BOSS-like survey up to  $k \approx 0.2 h\text{Mpc}^{-1}$ , for different halo mass bins.

Model	bin 1	bin 2	bin 3	bin 4	bin 5	bin 6	bin 7	bin 8	bin 9
This work	0.38(0.54)	0.52(0.75)	0.51(0.75)	0.62(0.86)	0.53(0.70)	0.60(0.76)	0.32(0.34)	0.23(0.33)	0.46(1.3)
Saito et al.2009	0.34(0.43)	0.49(0.62)	0.45(0.78)	0.68(0.80)	0.67(0.61)	0.30(0.31)	0.32(0.35)	0.23(0.26)	0.50(0.95)
McDonald 2006	0.30(0.32)	0.51(0.51)	0.50(0.49)	0.71(0.74)	0.63(0.85)	0.50(0.77)	0.39(0.43)	0.22(0.26)	0.50(0.82)
4 free parameters	0.19(0.21)	0.27(0.28)	0.19(0.21)	0.20(0.20)	0.23(0.21)	0.30(0.31)	0.25(0.26)	0.22(0.26)	0.24(0.36)
linear theory	5.1 (13.4)	5.4 (15.7)	4.3 (15.4)	4.4 (15.6)	3.6 (18.9)	4.3 (23.3)	8.4 (35.8)	12.6(49.0)	19.8(71.0)

**Table 2.** Comparison of the different models as in Fig. 6, but the numbers in each row- and column are the reduced  $\chi^2$ -values ( $\chi_r^2$ ) for the best-fit power spectra of each model. The different columns are for the halo catalogs of different mass bins (see Table 1). To compute the reduced  $\chi^2$  values, we obtained the best-fit model up to  $k_{\text{max}} = 0.15 h\text{Mpc}^{-1}$  by fitting the model prediction to the simulation spectra assuming the errors for a BOSS-like survey, while the value in parenthesis is the value for  $k_{\text{max}} = 0.20$ . The degrees of freedom for the  $\chi^2$  fitting is: 58 or 78 in total for  $P_{hm}$  and  $P_{hh}$  for  $k_{\text{max}} = 0.15$  or  $0.2 h\text{Mpc}^{-1}$ , respectively, minus the number of model parameters (either 2, 3 or 4). Our model has 2 free parameters, the models “Saito et al. (2009)” and “McDonald (2006)” have 3 parameters, and the model “4 free parameters” has 4 parameters. The linear theory breaks down, but the different models of the nonlinear power spectra are equally acceptable for a BOSS-like survey.

slightly better due to more free parameters. Note that the reduced  $\chi^2$  value is smaller than unity, partly because the central values of the simulated spectra are taken from the simulations of  $22.5 (\text{Gpc}h^{-1})^3$  volume and therefore the central value have smaller scatters than expected from a BOSS-like survey.

## 5 SUMMARY AND DISCUSSION

In this paper, we have studied a method of modeling the nonlinear halo power spectra,  $P_{hm}(k)$  and  $P_{hh}(k)$ , by combining the PT approach of structure formation, the local bias ansatz and the halo bias. The nonlinearities of halo power spectra, which are deviations from the linear theory prediction, arise from the two effects: the nonlinear matter clustering and the nonlinear relation between

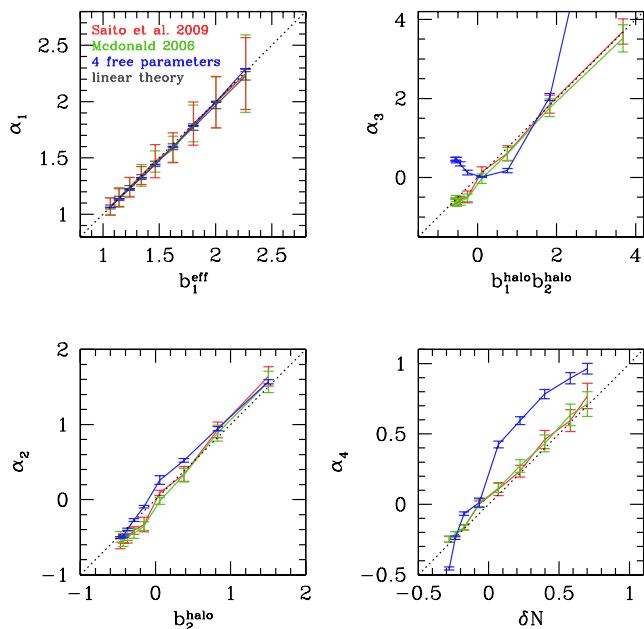


**Figure 7.** Comparison of the best-fit coefficients ( $\alpha_1$ ,  $\alpha_2$ ,  $\alpha_3$ ,  $\alpha_4$ ) in the model nonlinear power spectra (Eq. 22) with the best-fit parameters of our model, obtained from the 9 halo catalogs. Here we consider the different models as in Fig. 6 (also see below Eq. 22). Note that  $b_1(M)$  and  $b_2(M)$  in the  $x$ -axis of the upper-right or lower-left panels are the halo bias parameters for different halo mass bins. The best-fit parameters are obtained by using the power spectra  $P_{hm}$  and  $P_{hh}$  up to  $k = 0.2 \text{ hMpc}^{-1}$  for a BOSS-like survey, as in Fig. 6 or Table 2. The panels show that our model is almost equivalent to the models “Saito et al. (2009)” and “McDonald (2006)”, implying that the halo bias parameters are a good approximation for the forms of the nonlinear power spectra given by Eq. (22).

the matter and halo density fields. In deriving the nonlinear halo power spectra, we employed the renormalization approach (McDonald 2006) to re-sum the higher-order terms so that the terms are replaced with the nonlinear matter power spectrum, multiplied by the “renormalized” linear bias parameter. The remaining terms in the nonlinear halo spectra are given as a function of the linear matter power spectrum and the halo bias, where the terms at the one-loop correction order are included. As a result, we expressed the halo-matter cross-power spectrum (Eq. 13) in terms of the nonlinear and linear matter power spectra, the halo bias ( $b_2(M)$ ), and one free parameter, the renormalized linear bias parameter ( $b_1^{\text{eff}}$ ), which needs to be determined in the linear regime. Similarly, the halo auto-power spectrum (Eq. 14) is given as a function of the nonlinear and linear matter power spectra, the halo bias functions ( $b_1(M)$ ,  $b_2(M)$ ), and the two free parameters,  $b_1^{\text{eff}}$  and the residual shot noise parameter  $\delta N$ . Thus our method utilizes the recent development in an accurate model of the nonlinear matter power spectrum based on the refined perturbation theory and/or  $N$ -body simulations. In our model, the halo power spectra are specified by cosmological parameters, halo mass, redshift, and a less number of free parameters.

We showed that our model predictions for  $P_{hm}(k)$  and  $P_{hh}(k)$  are in nice agreement with the simulation results, up to  $k \approx 0.2 \text{ hMpc}^{-1}$ , at simulation output  $z = 0.35$  (see Figs. 3 and 4), if using the improved PT theory prediction for the nonlinear matter power spectrum in the model calculation. The linear power spectrum breaks down at  $k \approx 0.1 \text{ hMpc}^{-1}$ . Thus our model might allow a factor 2 gain in the maximum wavenumber  $k_{\text{max}}$  up to which to

include the power spectrum information when constraining cosmological parameters. In the sampling variance limited regime, the factor 2 gain is equivalent to a factor 8 larger volume, yielding greater statistical power of the power spectrum measurement. In addition, a wider coverage of wavenumbers in the power spectrum amplitudes gives a higher sensitivity to some of intriguing cosmological parameters such as the total neutrino mass (Saito et al. 2008, 2009, 2011) and the running index of the primordial power spectrum. Thus developing a sufficiently accurate model of the nonlinear halo power spectrum is very important in order for us to have improved cosmological constraints, yet without having any significant biases in the derived parameters.

Our model naturally predicts that, in the weakly nonlinear regime, the halo power spectra show a scale-dependent bias relative to the nonlinear matter power spectrum (see Figs. 2 and 5). The PT based model naturally predicts that the two bias functions, defined as  $b^{\text{cross}}(k) = P_{hm}(k)/P_m(k)$  and  $b^{\text{auto}}(k) = \sqrt{P_{hh}(k)/P_m(k)}$ , differ in the weak nonlinear regime. Furthermore, by incorporating the halo occupation distribution (HOD) model, we can predict the nonlinear power spectra of galaxy-matter and galaxy-galaxy in the weakly nonlinear regime. We hope that our model can give a better description of the nonlinear galaxy power spectra, and then allows for improved cosmological constraints via the measured power spectra. Our model can be further refined by including the higher-order loop corrections to the nonlinear bias functions.

We showed that our model using the halo bias can give a good fit to the simulation results for the halo spectra. This offers a promising synergy between imaging and spectroscopic galaxy surveys, because a cross-correlation of the spectroscopic galaxies with images of background galaxies, the so-called galaxy-galaxy weak lensing, can directly probe the mean mass of host halos and in turn constrain the halo bias. Here the halo mass is constrained from the small-scale weak lensing signals arising from the mass distribution within one halo, which is complementary to the large-scale information of galaxy clustering at  $k \lesssim 0.2 \text{ hMpc}^{-1}$  we focus on in this paper. This synergy is available if the spectroscopic and imaging surveys see the same region of the sky. This is the case for upcoming surveys: the BOSS and the Subaru HSC Survey, the Subaru HSC and PFS surveys, the Euclid, the WFIRST and a combination of the LSST survey with spectroscopic surveys.

However, our method rests on simplified assumptions one of which is the local bias model. Our model can be further improved by including the non-locality of halo bias such as the dependence of halo bias on the curvature of the initial density peaks (Desjacques et al. 2010) and/or the tidal field around the density peaks (Chan et al. 2012; Baldauf et al. 2012). This is an interesting possibility, and will be explored in our future work.

In this paper, we have focused on the real-space power spectra of halos or galaxies. Actual observable for galaxy redshift survey is the redshift-space power spectrum of galaxies, which is affected by the redshift-space distortion effect due to peculiar motions of galaxies. Towards a more accurate modeling of the nonlinear galaxy power spectrum in redshift space, we need to further include the nonlinear coupling between the redshift-space distortion effect and the nonlinear galaxy bias. There are encouraging developments in modeling the redshift-space matter power spectrum in redshift-space, based on the refined perturbation theory and  $N$ -body simulations (Matsubara 2008b; Taruya et al. 2009, 2010; Tang et al. 2011; Matsubara 2011; Sato & Matsubara 2011). The redshift-space distortion effect due to virial motions of galaxies within halos, the so-called Fingers-of-God (FoG) effect, is harder to model, but Hikage et al. (2012b,a) recently developed an empir-

ical method to model the FoG effect based on the halo model and proposed a method to remove the FoG contamination by combining with galaxy-galaxy weak lensing measurement. It seems straightforward to incorporate these methods in the method developed in this paper, in order to include all the effects, nonlinear clustering, nonlinear bias, nonlinear redshift-space distortion and FoG effect. This is our future work and will be presented elsewhere. These efforts are very important in order to attain the full potential of future high-precision galaxy surveys as well as to obtain unbiased, robust cosmological constraints from the surveys.

## ACKNOWLEDGEMENTS

We thank Issha Kayo, Ravi Sheth and Atsushi Taruya for useful discussion. In particular, we thank Atsushi Taruya for making the code to compute the nonlinear matter power spectrum publicly available to us. This work is supported in part by the Grant-in-Aid for the Scientific Research Fund (No. 23340061), by JSPS Core-to-Core Program “International Research Network for Dark Energy”, by World Premier International Research Center Initiative (WPI Initiative), MEXT, Japan, and by the FIRST program “Subaru Measurements of Images and Redshifts (SuMIRE)”, CSTP, Japan. T. N. is supported by a Grant-in-Aid for Japan Society for the Promotion of Science (JSPS) Fellows (PD: 22-181).

## REFERENCES

- Angulo R. E., Baugh C. M., Frenk C. S., Lacey C. G., 2008, *MNRAS*, 383, 755
- Baldauf T., Seljak U., Desjacques V., McDonald P., 2012, *Phys. Rev. D*, 86, 083540
- Baldauf T., Smith R. E., Seljak U., Mandelbaum R., 2010a, *Phys. Rev. D*, 81, 063531
- Baldauf T., Smith R. E., Seljak U., Mandelbaum R., 2010b, *Phys. Rev. D*, 81, 063531
- Bernardeau F., Colombi S., Gaztañaga E., Scoccimarro R., 2002, *Phys. Rep.*, 367, 1
- Chan K. C., Scoccimarro R., Sheth R. K., 2012, *Phys. Rev. D*, 85, 083509
- Coles P., 1993, *MNRAS*, 262, 1065
- Cooray A., Sheth R., 2002, *Phys. Rep.*, 372, 1
- Crocce M., Scoccimarro R., 2006, *Phys. Rev. D*, 73, 063519
- Desjacques V., Crocce M., Scoccimarro R., Sheth R. K., 2010, *Phys. Rev. D*, 82, 103529
- Desjacques V., Jeong D., Schmidt F., 2011, *Phys. Rev. D*, 84, 063512
- Fry J. N., 1984, *ApJ*, 279, 499
- Fry J. N., Gaztanaga E., 1993, *ApJ*, 413, 447
- Goroff M. H., Grinstein B., Rey S.-J., Wise M. B., 1986, *ApJ*, 311, 6
- Hamaus N., Seljak U., Desjacques V., 2011, *Phys. Rev. D*, 84, 083509
- Heavens A. F., Matarrese S., Verde L., 1998, *MNRAS*, 301, 797
- Hikage C., Mandelbaum R., Takada M., Spergel D. N., 2012a, *ArXiv:1211.1009*
- Hikage C., Takada M., Spergel D. N., 2012b, *MNRAS*, 419, 3457
- Hu W., Kravtsov A. V., 2003, *ApJ*, 584, 702
- Jain B., Bertschinger E., 1994, *ApJ*, 431, 495
- Jeong D., Komatsu E., 2006, *ApJ*, 651, 619
- Jeong D., Komatsu E., 2009, *ApJ*, 691, 569
- Juszkiewicz R., 1981, *MNRAS*, 197, 931
- Kaiser N., 1984, *ApJ Lett.*, 284, L9
- Komatsu E. et al., 2011, *ApJS*, 192, 18
- Makino N., Sasaki M., Suto Y., 1992, *Phys. Rev. D*, 46, 585
- Mandelbaum R., Slosar A., Baldauf T., Seljak U., Hirata C. M., Nakajima R., Reyes R., Smith R. E., 2012, *ArXiv:1207.1120*
- Manera M., Sheth R. K., Scoccimarro R., 2010, *MNRAS*, 402, 589
- Matsubara T., 1999, *ApJ*, 525, 543
- Matsubara T., 2008a, *Phys. Rev. D*, 78, 083519
- Matsubara T., 2008b, *Phys. Rev. D*, 77, 063530
- Matsubara T., 2011, *Phys. Rev. D*, 83, 083518
- McDonald P., 2006, *Phys. Rev. D*, 74, 103512
- McDonald P., Roy A., 2009, *JCAP*, 8, 20
- Mo H. J., White S. D. M., 1996, *MNRAS*, 282, 347
- Navarro J. F., Frenk C. S., White S. D. M., 1997, *ApJ*, 490, 493
- Nishimichi T. et al., 2007, *PASJ*, 59, 1049
- Nishimichi T. et al., 2009, *PASJ*, 61, 321
- Nishimichi T., Taruya A., 2011, *Phys. Rev. D*, 84, 043526
- Oguri M., Takada M., 2011, *Phys. Rev. D*, 83, 023008
- Peacock J. A., Smith R. E., 2000, *MNRAS*, 318, 1144
- Pollack J. E., Smith R. E., Porciani C., 2012, *MNRAS*, 420, 3469
- Reid B. A. et al., 2010, *MNRAS*, 404, 60
- Reid B. A., Spergel D. N., 2009, *ApJ*, 698, 143
- Reid B. A., Spergel D. N., Bode P., 2009, *ApJ*, 702, 249
- Saito S., Takada M., Taruya A., 2008, *Physical Review Letters*, 100, 191301
- Saito S., Takada M., Taruya A., 2009, *Phys. Rev. D*, 80, 083528
- Saito S., Takada M., Taruya A., 2011, *Phys. Rev. D*, 83, 043529
- Sato M., Matsubara T., 2011, *Phys. Rev. D*, 84, 043501
- Scherrer R. J., Weinberg D. H., 1998, *ApJ*, 504, 607
- Schmidt F., Jeong D., Desjacques V., 2012, *ArXiv:1212.0868*
- Scoccimarro R., Hui L., Manera M., Chan K. C., 2012, *Phys. Rev. D*, 85, 083002
- Scoccimarro R., Sheth R. K., Hui L., Jain B., 2001, *ApJ*, 546, 20
- Seljak U., 2000, *MNRAS*, 318, 203
- Sheth R. K., Tormen G., 1999, *MNRAS*, 308, 119
- Springel V. et al., 2005, *Nature*, 435, 629
- Suto Y., Sasaki M., 1991, *Physical Review Letters*, 66, 264
- Takahashi R. et al., 2009, *ApJ*, 700, 479
- Tang J., Kayo I., Takada M., 2011, *MNRAS*, 416, 2291
- Taruya A., Hiramatsu T., 2008, *ApJ*, 674, 617
- Taruya A., Nishimichi T., Saito S., 2010, *Phys. Rev. D*, 82, 063522
- Taruya A., Nishimichi T., Saito S., Hiramatsu T., 2009, *Phys. Rev. D*, 80, 123503
- Taruya A., Suto Y., 2000, *ApJ*, 542, 559
- Tinker J., Kravtsov A. V., Klypin A., Abazajian K., Warren M., Yepes G., Gottlöber S., Holz D. E., 2008, *ApJ*, 688, 709
- Valageas P., Nishimichi T., 2011, *Astronomy & Astrophysics*, 527, A87
- Vishniac E. T., 1983, *MNRAS*, 203, 345
- White M., 2002, *Astrophys. J. Suppl.*, 143, 241